

CO₂ Hydrogenation to CH₃OH over PdZn Catalysts, with Reduced CH₄ Production

Jonathan Ruiz Esquiús,^[a] Hasliza Bahruji,^[a, b] Stuart H. Taylor,^[a] Michael Bowker,^{*,[a, c]} and Graham J. Hutchings^{*,[a]}

Metallic Pd, under CO₂ hydrogenation conditions (> 175 °C, 20 bar in this work), promotes CO formation *via* the reverse water gas shift (RWGS) reaction. Pd-based catalysts can show high selectivity to methanol when alloyed with Zn, and PdZn alloy catalysts are commonly reported as a stable alternative to Cu-based catalysts for the CO₂ hydrogenation to methanol. The production of CH₄ is sometimes reported as a minor by-product, but nevertheless this can be a major detriment for an industrial process, because methane builds up in the recycle loop, and hence would have to be purged periodically. Thus, it is extremely important to reduce methane production for future

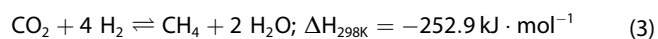
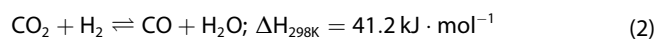
green methanol synthesis processes. In this work we have investigated TiO₂ as a support for such catalysts, with Pd, or PdZn deposited by chemical vapour impregnation (CVI). Although titania-supported PdZn materials show excellent performance, with high selectivity to CH₃OH + CO, they suffer from methane formation (> 0.01 %). However, when ZnTiO₃ is used instead as a support medium for the PdZn alloy, methane production is greatly suppressed. The site for methane production appears to be the TiO₂, which reduces methanol to methane at anion vacancy sites.

Introduction

Currently, over 85% of global energy is obtained from finite resources (coal, oil or natural gas), giving increased atmospheric CO₂ levels^[1] and inevitable climate change consequences.^[2] Economic growth has in the past been associated with the availability of finite resources for the production of energy.^[3] The specific location of natural resources and their fluctuating price has resulted in intergovernmental frictions,^[4] which are expected to intensify as the cheapest natural deposits deplete over time. Hence, the production of energy from renewables is one of the biggest challenges to secure a steady energy supply

and to tackle global CO₂ emissions. Current technology (e.g., wind and solar farms, hydroelectric power stations) allows the production of electricity free of carbon emissions. The main drawback for renewable electricity is its intermittent nature, which therefore requires some method of storage of this energy when production is high, to be used when production is low. Currently the most efficient and industrially scalable route to store renewably-produced electricity is through water splitting to produce H₂, so-called green hydrogen.^[5] Hydrogen can be used as an energy vector, however, it has a low energy density per volume, and most current technology has evolved around much more energy-dense molecules. Hence, to readily incorporate green hydrogen into conventional technology, it may be necessary to convert it to a liquid fuel. One possible route is to transform it into methanol by its reaction with captured CO₂, which in turn will alleviate carbon dioxide emissions.

The selective CO₂ hydrogenation to CH₃OH (Equation 1) is challenging because of the possibility of simultaneous reactions occurring, such as the reverse water gas shift (RWGS) (Equation 2) and methanation (Equation 3), which produce CO and CH₄ respectively. Thermodynamically, the production of CH₃OH and CH₄ are favoured at low temperature and high pressure, while high temperature promotes the RWGS.



In a methanol plant, liquid products (CH₃OH and H₂O) are separated from gaseous products through some form of condenser, unreacted reagents (CO₂ and H₂) and gaseous products (CO and CH₄) are recycled into the catalyst bed.^[6] The

[a] Dr. J. Ruiz Esquiús, Dr. H. Bahruji, Prof. Dr. S. H. Taylor, Prof. M. Bowker, Prof. G. J. Hutchings
School of Chemistry
Cardiff Catalysis Institute
Cardiff University
Main Building
Park Place
Cardiff CF10 3AT (UK)
E-mail: BowkerM@cardiff.ac.uk
Hutch@cardiff.ac.uk

[b] Dr. H. Bahruji
Centre of Advanced Material and Energy Science
University Brunei Darussalam
Jalan Tungku Link
Gadong, BE 1410 (Brunei Darussalam)

[c] Prof. M. Bowker
Catalysis Hub, RCAH
Rutherford Appleton Laboratory
Harwell Oxford
Didcot OX11 0QX (UK)

Supporting information for this article is available on the WWW under <https://doi.org/10.1002/cctc.202000974>

© 2020 The Authors. Published by Wiley-VCH GmbH. This is an open access article under the terms of the Creative Commons Attribution License, which permits use, distribution and reproduction in any medium, provided the original work is properly cited.

formation of CO is not detrimental for the overall process, since carbon monoxide can also be transformed to CO₂ or methanol, moreover, the presence of CO in the gas feed can result in enhanced methanol yield.^[7] However, CH₄ accumulates during gas recycling cycles, and eventually needs to be purged, increasing production costs.

Copper based catalysts are commonly employed for the CO₂ hydrogenation to CH₃OH, however strong Cu-sintering^[8–11] and coke deposition^[12] are observed when CO₂ is used as the feed. Noble-metal based catalysts can be used to overcome the catalyst deactivation observed with Cu-based catalysts, with the PdZn alloy system being one of the materials receiving research attention. Iwasa *et al.*^[13] showed that on Pd-based catalysts at ambient pressure, the support controls the product selectivity. Over palladium black, CO₂ reacts with H₂ at atmospheric pressure to form primarily CO and CH₄, with no CH₃OH formation. Supports with little interaction with palladium (SiO₂ or MgO) formed no methanol, while over supports that can form alloys or intermetallics with palladium upon reduction (e.g. ZnO and Ga₂O₃) methanol selectivity significantly increased. For PdZn, the change in product selectivity can be associated to an electron density distribution from the electron rich Pd(4d) to external Pd(5s), Pd(5p) and Zn(4p), Zn(4s) orbitals.^[14] Díez-Ramírez *et al.*^[15,16] and Bahruji *et al.*^[17] in separate studies over Pd/ZnO catalysts confirmed that the PdZn alloy phase, formed upon pre-reduction in hydrogen at high temperature (>300 °C), acts as the active phase for methanol synthesis. On Pd/ZnO catalysts, the PdZn alloy phase is also active for the formation of CO,^[18] whilst metallic Pd sites are responsible for CO^[16] and CH₄ formation.^[19,20]

CH₄ is commonly reported as a minor side product on PdZn alloy catalysts.^[13,15,21,22] However, not much attention is paid to CH₄ because of its low selectivity (less than 1%), which can lead to the misinterpretation that it is not important and that CH₄ formation is inherent to PdZn catalysts. This could limit applications of PdZn based catalysts in a CH₃OH synthesis plant operating with captured CO₂ and green hydrogen. For comparison purposes, Table S1 shows CH₄ productivity and selectivity reported for Pd-based catalysts employed as CH₃OH synthesis catalysts.

During the CO₂ hydrogenation on a PdZn/TiO₂ catalyst, methanol is formed over PdZn surfaces,^[15,16,23] CO can be produced over metallic Pd^[13,15,24] or PdZn,^[25] however, little is known about the active sites for CH₄ formation on PdZn alloys. In this work, it is proposed that over PdZn/TiO₂ catalysts CH₄ is not formed through the methanation of CO₂, but instead as a by-product of CH₃OH decomposition at TiO₂ sites.

Experimental Section

Materials

All materials used in this work were purchased from Sigma Aldrich; palladium acetylacetonate (Pd(acac)₂, 99%), zinc acetylacetonate (Zn(acac)₂, 99%), ZnO (nanopowder, <100 nm particle size) and TiO₂ (P25, aereoxide).

ZnTiO₃ synthesis

Rhombohedral ZnTiO₃ (3 g) was prepared as follows; Zn(acac)₂ (5.40 g, 18 mmol) and TiO₂ (1.50 g, 18 mmol) were physically mixed inside a glass vial for 1 min. The mixture was transferred to a Schlenk flask, evacuated (10⁻³ bar) and heated (145 °C, 1 h). Afterwards, the pre-catalyst was recovered, annealed (static air, 500 °C, 10 °C·min⁻¹, 16 h) and reduced (5% H₂, 650 °C, 5 °C min⁻¹, 3 h). The XRD pattern for the synthesised ZnTiO₃ is included in Figure S1.

Catalyst synthesis

Chemical vapour impregnation (CVI) was employed as the synthetic methodology because it presents several advantages over conventional wet preparation routes. It allows the preparation of highly dispersed small nanoparticles, it avoids contamination from the use of solvents or ligands, avoids chlorine contamination, which can be detrimental for CO₂ hydrogenation activity and it allows the easy preparation of bimetallic catalysts.^[26–28]

Catalyst were prepared by chemical vapour impregnation (CVI) with a 5 wt. % Pd loading; For the preparation of PdZn/ZnTiO₃ and PdZn/TiO₂ catalysts (2 g, Pd:Zn molar ratio of 1:5) Pd(acac)₂ (0.28 g, 9.4·10⁻⁴ mol), Zn(acac)₂ (1.11 g, 4.7·10⁻³ mol) and 1.6 g ZnTiO₃ or TiO₂ were physically mixed in a glass vial for 1 min. The mixture was transferred to a Schlenk flask, evacuated (10⁻³ bar) and heated (145 °C, 1 h). The material was recovered and annealed in static air at (500 °C, 10 °C min⁻¹, 16 h). For the preparation of Pd/ZnTiO₃, Pd/TiO₂ or Pd/ZnO catalysts (2 g) Pd(acac)₂ (0.28 g, 9.4·10⁻⁴ mol) and 1.9 g of support (ZnTiO₃, TiO₂ or ZnO respectively) were physically mixed for 1 min in a glass vial. The mixture was transferred into a Schlenk flask, evacuated (10⁻³ bar), and heated (145 °C, 1 h). The material was recovered and annealed in static air at (500 °C, 10 °C min⁻¹, 16 h). They were pre-reduced (400 °C, H₂, 1 h) and tested for CO₂ hydrogenation in a flow reactor between 175 °C and 250 °C (20% CO₂, 20% N₂, 60% H₂, 20 bar, 30 mlmin⁻¹, 0.5 g_{cat}).

Characterisation was performed on a portion of the catalyst reduced in 5% H₂/Ar (400 °C, 1 h, 10 mL min⁻¹).

Catalyst characterisation

Powder X-ray diffraction (XRD) patterns were recorded on a (θ-θ) PANalyticalX'pert Pro powder diffractometer fitted with a position sensitive detector using Cu Kα radiation source (40 keV, 40 mA). *In situ* XRD was recorded on a (θ-θ) PANalyticalX'pert Pro powder diffractometer fitted with a position sensitive detector using a Cu Kα radiation source (40 keV, 40 mA) and an Anton Parr XRK reaction cell connected to a 5% H₂/Ar mixture, gas flow was controlled through the use of a Bronkhorst mass flow controller.

X-ray photoelectron spectroscopy (XPS) was carried out on a Kratos Axis Ultra-DLD fitted with a monochromatic Al Kα (75–150 W) source and an analyser using a pass energy of 40 eV. XPS data were analysed using Casa XPS software.

Transmission electron microscopy images were obtained on a JEOL 2100 (LaB6) instrument fitted with a Gatan digital camera (2k 2k) and a dark held HAADF/Z-contrast detector. Specimens were dry-prepared on copper TEM-grids prior to analysis, to obtain representative particle size distributions at least 200 particles were analysed.

BET surface areas were measured using a Quantachrome Nova 2200e instrument. Prior to BET analysis samples were degassed in situ (120 °C, 4 h).

CO₂ hydrogenation catalyst testing

The catalyst activity for CO₂ hydrogenation was measured in a stainless steel fixed-bed (50 cm length, 0.5 cm internal diameter) continuous flow reactor. 0.5 g of pelleted then crushed (425–600 μm) catalyst was placed in the reactor tube without diluent, quartz wool was used to secure the catalyst bed in place. Reaction temperature was controlled through a chromel-alumel thermocouple placed in the catalyst bed. Prior to reaction, catalysts were pre-reduced in pure hydrogen (400 °C, 5 °C min⁻¹, 1 h, 30 ml min⁻¹). Subsequently, the reactor was cooled to 50 °C, the gas flow was switched from hydrogen to the reaction mixture (20 % CO₂, 20 % N₂, 60 % H₂, 30 ml min⁻¹), pressurised to 20 bar and heated to the desired reaction temperature (175–250 °C, 5 °C min⁻¹). Post reactor lines and valves were heated at 130 °C to avoid product condensation. Products were analysed *via* online gas chromatography (Agilent 7890, fitted with a FID and TCD detectors). Details of how to determine reaction metrics (CO₂ conversion, product selectivity and productivities) can be found in the supporting information (equation S1–S9).

Results and Discussion

Catalytic activity for the thermal CO₂ hydrogenation

Previously we have shown that the synthesis of PdZn alloys prepared by chemical vapour impregnation (CVI) using TiO₂ as support gave improved PdZn dispersion compared to the use of ZnO and Al₂O₃, and resulted in improved methanol production rates.^[29] However, during the CO₂ hydrogenation (250 °C, 20 bar) over 5 wt. % PdZn(1:5)/TiO₂, CH₄ formation was observed at 0.1 % selectivity.^[30] Although this may seem like a small amount of this by-product, it nevertheless would result in increased production costs due to the need to purge it after build-up in the recycle system. Hence it is important to minimise CH₄ formation, and to try to identify the exact source for this product. The concentration of active sites for CH₄ formation decreased after increasing the pre-reduction temperature from 400 °C to 650 °C, which was associated with Zn incorporation into the TiO₂ lattice forming ZnTiO₃. To determine the active sites responsible for CH₄ formation Pd/TiO₂, Pd/ZnO, Pd/ZnTiO₃, PdZn/TiO₂ and PdZn/ZnTiO₃ catalysts were prepared by CVI as described above.

On catalysts containing Pd, CO₂ in the presence of H₂ is converted into CO *via* the RWGS,^[13,24] but as we show below, CH₄ can be a by-product of reaction. On Pd-based catalysts employed for the methanation of CO₂, debate remains about whether CO is reduced at the metal-support interface^[19] or on Pd nanoparticles.^[31] As shown in Table 1, the lowest methanol

productivity is found for Pd/TiO₂, whilst it showed the highest CH₄ productivity, in agreement with previous reports on Pd-based catalysts.^[20,31,32] Prior to reaction, catalysts were pre-reduced (400 °C, H₂, 1 h) to form the PdZn active phase for methanol synthesis.^[17,30,33,34] As observed for Pd/ZnO, Pd/ZnTiO₃, PdZn/TiO₂ and PdZn/ZnTiO₃ the formation of β-PdZn resulted in enhanced methanol selectivity compared to Pd/TiO₂ throughout the temperature range studied (Table S2). CO₂ is a relatively stable molecule, and high reaction temperature is required for its activation. Increasing reaction temperature resulted in higher CO₂ conversion, however, methanol synthesis is favoured at low temperature and high pressure,^[7] hence the decrease in methanol selectivity, seen for instance in figure 1 for Pd/ZnO, in favour to CO production *via* the RWGS reaction with increasing temperature.

At 250 °C no CH₄ was produced within the detection limits of the GC-FID (1 ppm or ~0.0005 % effective yield) for Pd/ZnO, where Pd is present as PdZn. Alongside Pd/ZnO, no significant CH₄ formation was observed for PdZn/ZnTiO₃ below 250 °C (X CO₂ ~ 13 %) (Figure 2). Indicating that CH₄ formation does not occur on ZnO, ZnTiO₃, PdZn alloy facets or the combination of these. On PdZn/TiO₂, CH₄ formation was observed at 200 °C, CH₄ productivity increased with increasing reaction temperature, reaching a productivity of 0.5 mmol Kg_{cat}⁻¹ h⁻¹ at 250 °C (X CO₂ ~ 12 %). Indicating that TiO₂ is most probably involved in the production of CH₄. Others suggest that CH₄ can be formed through a CO₂ methanation mechanism, at either Pd surfaces,^[31] or via carbonate intermediates formed on TiO₂^[35] and further hydrogenation at the metal-support interface.^[19] Another plausible mechanism for CH₄ production on PdZn catalysts is the migration of adsorbed methanol molecules, originating at the PdZn phase, to TiO₂, where it decomposes *via* methoxide deoxygenation and methyl-hydrogenation.^[36,37] On Pd/ZnTiO₃, CH₄ production followed the same CO₂ conversion/CH₄ productivity trend as PdZn/TiO₂ (Figure 2). Blank test for CO₂ hydrogenation, under the same reaction conditions used for PdZn catalysts, using TiO₂, ZnO and ZnTiO₃ supports, showed very little conversion, as might be expected (Table S3). To discern whether on PdZn catalysts CH₄ is formed through CO₂ methanation or *via* CH₃OH decomposition, a physical mixture of Pd/ZnO and TiO₂ was used for the CO₂ hydrogenation (Table S4). At 250 °C, a CH₄ productivity of 1.8 mmol Kg_{cat}⁻¹ h⁻¹ was observed. Firstly, this indicates that CH₄ is formed over the Pd/ZnO physical mixture *via* CH₃OH decomposition, and not through CO₂ methanation as reported for Pd catalysts,^[38] and secondly, that CH₃OH can adsorb and decompose at TiO₂ surfaces, and not exclusively at the PdZn-support interface.

Table 1. Catalytic performance for thermal CO₂ hydrogenation (20 % CO₂, 20 % N₂, 60 % H₂, 30 ml min⁻¹, 20 bar, 225 °C) obtained for 5 wt. % Pd catalysts prepared by CVI after annealing in static air (500 °C, 16 h) followed by *in situ* pre-reduction in pure H₂ (400 °C, 1 h, 5 °C min⁻¹, 30 ml min⁻¹).

Catalyst	X CO ₂ [%]	CH ₃ OH sel. [%]	CO sel. [%]	CH ₄ sel. [%]	CH ₃ OH prod. [mmol Kg ⁻¹ h ⁻¹]	CO prod. [mmol Kg ⁻¹ h ⁻¹]	CH ₄ prod. [mmol Kg ⁻¹ h ⁻¹]
Pd/TiO ₂	8.7	8.5	90.3	0.9	201	2155	22
Pd/ZnO	6.5	30.2	69.8	0.000	561	1216	0.0
PdZn/TiO ₂	7.1	33.5	66.5	1 × 10 ⁻²	654	1297	0.2
Pd/ZnTiO ₃	6.1	40.2	59.8	5 × 10 ⁻³	683	1002	0.1
PdZn/ZnTiO ₃	7.5	38.7	61.3	0.000	797	1263	0.0

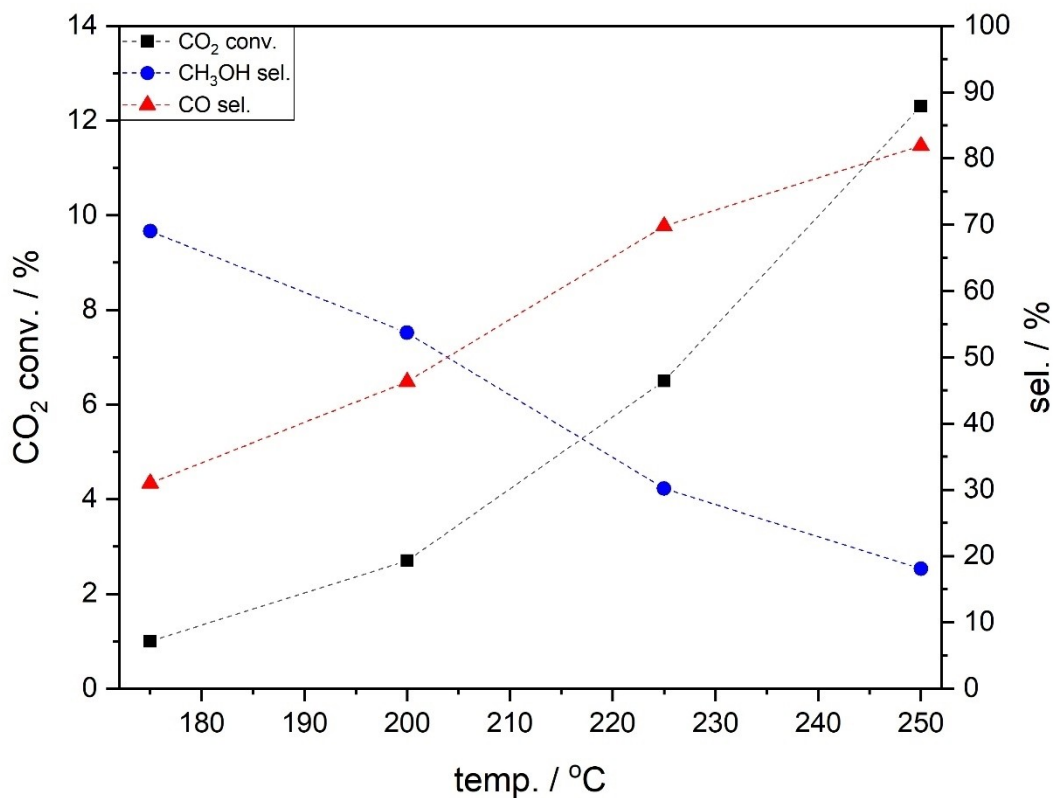


Figure 1. CO₂ conversion and change in the CH₃OH and CO selectivity with reaction temperature for Pd/ZnO (20 bar, CO₂:H₂:N₂ 1:3:1, 30 ml min⁻¹).

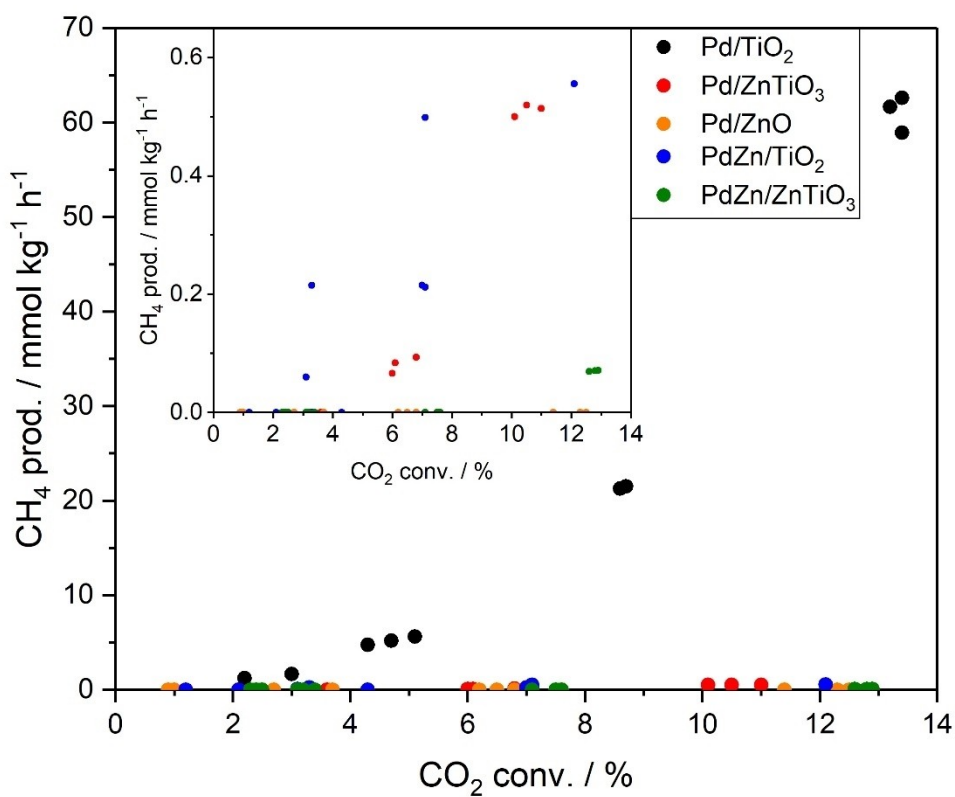


Figure 2. CH₄ productivity plotted against CO₂ conversion for PdZn/ZnTiO₃, Pd/ZnTiO₃, PdZn/TiO₂ and Pd/TiO₂ catalysts synthesised by CVI. Reaction conditions: 20% CO₂, 20% N₂, 60% H₂, 30 min min⁻¹, 20 bar. Insert: comparison between catalysts at low CH₄ production rates (< 1 mmol_{CH₄} kg_{cat}⁻¹ h⁻¹).

From this observation, it can be concluded that over Pd-based catalysts CH₄ can be produced from CO₂ methanation over unalloyed Pd as well as from CH₃OH decomposition over the support, in this instance TiO₂. This highlights the importance of carefully considering the support to avoid CH₄ formation, even in trace amounts.

Chemical, structural and morphological catalyst characterisation

ZnO, TiO₂ and ZnTiO₃, with respective BET surface areas of 15 m²g⁻¹, 50 m²g⁻¹ and 17 m²g⁻¹, were used as supports for Pd or PdZn. In view of the high loading of 5 wt.% of Pd and 15 wt.% of Zn, the BET surface area of prepared catalysts after annealing (500 °C, 16 h) and pre-reduction (400 °C, 1 h) was measured. As shown in Table 2, the BET surface areas of the catalysts were comparable to the BET surface areas of the supports, indicating that most of the organic part of the organometallic precursor had decomposed without being deposited at the surface. Highly dispersed PdZn nanoparticles are desired for CO₂ hydrogenation to methanol, because of the improved metal surface area, and the surface area of the support employed is expected to affect the catalyst dispersion and its particle size distribution.^[29] However, no significant differences in the average particle size were observed by TEM between PdZn catalysts supported on TiO₂, ZnO or ZnTiO₃ (Table 2). Nevertheless, particle size histograms for PdZn/TiO₂ and PdZn/ZnTiO₃, where Pd(acac)₂ and Zn(acac)₂ were impregnated on the support, showed a narrower particle size distribution with a lower frequency of larger nanoparticles (> 7 nm) compared to Pd/ZnO and Pd/ZnTiO₃, where only Pd(acac)₂ was impregnated on the support (Figure S2). TEM images for the synthesised catalysts can be found in Figure S3.

CVI was employed for the synthesis of Pd/TiO₂, Pd/ZnO, Pd/ZnTiO₃, PdZn/TiO₂ and PdZn/ZnTiO₃. After annealing in air (500 °C, 16 h), the decomposition of the organometallic precursors, Pd(acac)₂ and Zn(acac)₂, led to the formation of PdO and ZnO respectively (see XRD Figure S4a). A peak at 33.9° for PdO (JCPDS-041-1107) was observed for all catalysts, whilst ZnO, originating from Zn(acac)₂ decomposition, was detected at 31.8°, 34.4° and 36.2° for PdZn/TiO₂ and PdZn/ZnTiO₃. Reduc-

tion treatment prior to reaction is required to form the β-PdZn alloy. Previous reports,^[33,39,40] suggested that under reducing conditions, PdO is first reduced to Pd metal, followed by hydrogen spill over from Pd to adjacent ZnO, leading to oxide reduction and the formation of the β-PdZn alloy.^[39,41] The alloy formation mechanism under reducing conditions (5 % H₂/Ar) was confirmed by *in situ* XRD for Pd/ZnO (Figure 3). A decrease in the intensity of the peak at 33.9°, which is assigned to PdO, is observed with increasing reduction temperature from 50 °C to 210 °C, and appears to be complete by the latter temperature. At this temperature, the formation of Pd⁰ is detected at 39.9° (JCPDS-046-1043). The peak assigned to metallic palladium remains stable under reducing conditions until 325 °C, when a shoulder at 41.4° appears, indicating the incorporation of zinc into the palladium lattice to form the β-PdZn alloy.^[40] Increasing the reduction temperature to 400 °C leads to the further alloying of Pd to PdZn, as indicated by the increase in intensity of the PdZn peak at 41.4°. PdZn formation on the synthesised catalysts is expected to follow the mechanism reported by Penner *et al.*,^[39] with PdZn formation starting at the surface of Pd, and growing from the surface inwards.

After reduction (400 °C, 1 h), (111) and (200) reflections, corresponding to β-PdZn, were detected at 41.4° and 44.1° respectively^[13,18] for Pd/ZnO, PdZn/TiO₂, Pd/ZnTiO₃ and PdZn/ZnTiO₃ (Figure S4b). The identification of the PdZn phase on Pd/ZnTiO₃ (Figure 4), indicated that zinc within the ZnTiO₃ lattice, migrated out of the structure and to the palladium surface forming the PdZn alloy, presumably generating a PdZn-TiO₂ interface locally, which then may be responsible for methanol decomposition to CH₄. For Pd/TiO₂, PdO was detected after annealing (500 °C, 16 h, static air), however, because of the absence of zinc in the material only metallic Pd was detected after pre-reduction (400 °C, 1 h, 5 % H₂/Ar) at 39.9° and 41.4° (Figure S4b).

To study the extent of palladium alloying after pre-reduction, catalysts were characterised by X-ray photoemission spectroscopy (XPS), figure 5. Even though catalysts were annealed in static air at 500 °C for 16 h to remove the acetylacetonate organic moiety of the organometallic precursors, carbon was detected after pre-reduction (400 °C, 1 h, 5 % H₂/Ar), hence, the rest of the elements analysed were calibrated against the adventitious C(1 s) signal at 284.8 eV binding energy (b.e.).^[42] The Pd(3d) peak for Pd/TiO₂ was centred at 334.9 eV,^[30,42] indicating the presence of metallic palladium. Thorough interpretation of Pd(3d) core-electrons is challenging due to the need to use symmetric and asymmetric peaks for Pd and PdO respectively, the presence of satellites and plasmon contributions.^[43] Finite-Lorentzian line shapes with Shirley background were used to fit Pd and PdZn main peaks and satellite contributions, whilst symmetric gaussian peaks were used to fit PdO main peaks and its satellites. Peak fitting on Pd/TiO₂ indicated the presence of PdO at 336.5 eV^[30,44,45] (Figure 5). PdO originated from the spontaneous Pd surface passivation in contact with air when transferred into the XPS instrument.^[46] For the reduced Pd/ZnO, a 1.2 eV shift towards higher binding energy is observed when compared to Pd/TiO₂, which indicates the incorporation of Zn within the lattice to form the PdZn

Table 2. 5 point BET surface area and PdZn particle size distribution obtained from TEM for 5 wt. % Pd catalysts prepared by CVI after annealing in static air (500 °C, 16 h), followed by pre-reduction in 5 % H₂/Ar (400 °C, 1 h).

Catalyst	BET surface area [m ² g ⁻¹]	Particle size [nm]
TiO ₂ ^[a]	50 ± 3	–
Pd/TiO ₂	48 ± 2	4.0 ± 1.3
PdZn/TiO ₂	44 ± 2	4.6 ± 0.9
ZnO ^[a]	15 ± 1	–
Pd/ZnO	14 ± 1	4.3 ± 1.8
ZnTiO ₃	17 ± 1	–
Pd/ZnTiO ₃	18 ± 1	6.4 ± 2.0
PdZn/ZnTiO ₃	21 ± 1	4.8 ± 1.2

[a] TiO₂ P25 and ZnO from Sigma Aldrich, used as support in the preparation of catalysts.

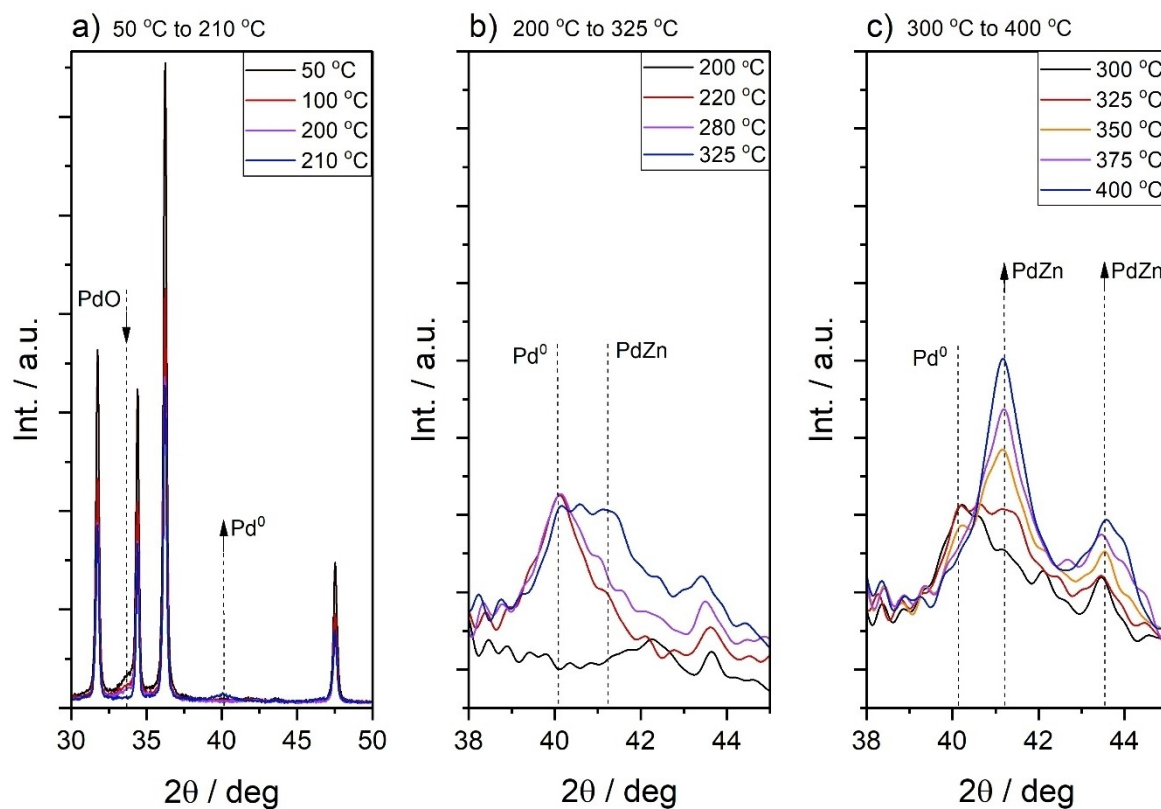


Figure 3. Transformation of PdO under reducing heat treatment (5% H₂/Ar, 25–400 °C) to Pd⁰ and PdZn alloy, followed by *in situ* XRD. To aid in phase transformations, *in situ* XRD patterns were arranged in three temperature ranges: a) from 50 to 210 °C, b) from 200 to 325 °C and c) from 300 to 400 °C.

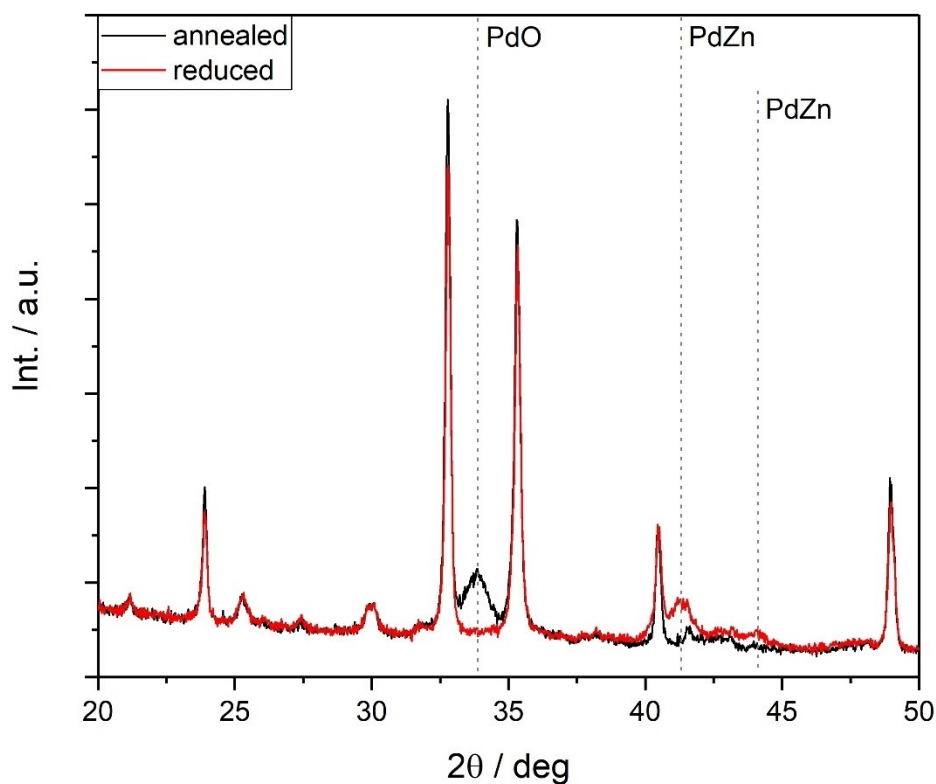


Figure 4. XRD pattern for Pd/ZnTiO₃ synthesised by CVI after annealing in air (500 °C, 16 h) and followed by reduction in 5% H₂/Ar (400 °C, 1 h).

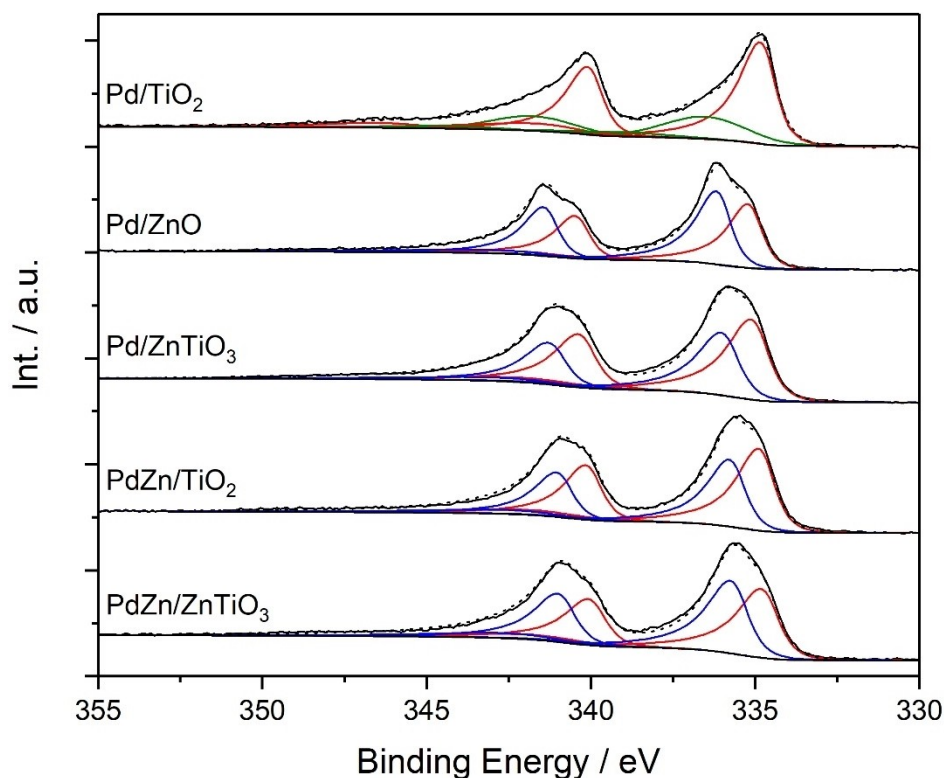


Figure 5. Pd(3d) XPS for CVI-synthesised catalysts after air annealing and subsequent reduction. Pd, PdZn and PdO in the peak fitting are represented in red, blue and green lines respectively. The fitting envelope is represented by a black-dotted line, while black solid line represents the recorded spectra.

alloy,^[30,41,47,48] in excellent agreement with the XRD characterisation. A part of PdZn at 336.1 eV, peak fitting suggested the presence of non-alloyed Pd at 335.1 eV, without a clear presence of PdO (Figure 5). The slight shift towards higher b.e. observed on the non-alloyed Pd peak for PdZn catalysts compared to Pd/TiO₂ can be attributed to stronger metal-support interactions^[33] and to atomic Zn-doping onto metallic Pd.^[49] As discussed for Pd/TiO₂, PdO is formed through oxidation of surface Pd in contact with air, however, alloyed palladium seems to be passivated against oxidation at room temperature when exposed to air. Metallic Pd is believed to be underneath a PdZn alloy layer, according to the PdZn alloy formation mechanism described in the literature,^[39] where PdO first reduces to Pd, and further reduction resulted in Zn incorporation into the Pd lattice leading to PdZn alloy, as observed by *in situ* XRD. The Pd(3d) peaks for Pd/ZnTiO₃, PdZn/ZnTiO₃ and PdZn/TiO₂ were shifted towards higher binding energy compared to Pd/TiO₂, in agreement with the formation of PdZn alloy as observed by XRD, peak fitting indicated the co-existence of PdZn and non-alloyed Pd in all catalysts (Figure 5), the latter presumably at the core of PdZn nanoparticles.^[39]

Changes in zinc speciation are challenging to detect by standard XPS because of the small change in the Zn(2p) binding energy upon oxidation. For instance, Zn metal and ZnO are reported at 1021.7 eV and 1022.0 eV respectively.^[42] No significant changes in the Zn(2p) b.e. were observed between synthesised catalysts (Figure S5a). The Zn(LM₂) Auger peak for

zinc oxide is at 988 eV with a minor satellite contribution at 991 eV,^[50] whilst for metallic zinc these peaks are much more shifted than the core levels, to 992 eV and 996 eV respectively.^[51] Therefore, the Zn(LM₂) Auger electron spectra were also analysed, since it has higher discrimination for chemical changes (Figure S5b). For Pd/ZnO, the two main peaks of ZnO were observed at 988 eV and 991 eV, as expected, but a shoulder, indicating the presence of zinc in a more reduced state than ZnO, was also observed at 995 eV,^[52] which can be assigned to Zn⁰ in the PdZn alloy.^[29] The presence of PdZn in the Zn(LM₂) Auger electron region was also observed for Pd/ZnTiO₃, PdZn/ZnTiO₃ and PdZn/TiO₂. Although there is very little metal in the spectra, it is likely that, at least some of the metallic zinc is oxidised upon exposure to air before the XPS. It is interesting to see that the Pd in the alloys does not oxidise significantly (figure 4), indicating that either it is covered by ZnO, possibly due to air exposure, or that it is passivated by it.

In summary our study shows that by careful control of the preparation method and selection of a suitable support, PdZn alloy catalysts can be synthesised that can hydrogenate CO₂ to methanol without the formation of CH₄, which is an undesired product from a production viewpoint.

Conclusions

The synthesis of a range of Pd and PdZn catalysts supported on TiO₂, ZnO and ZnTiO₃ by chemical vapour impregnation allowed us to confirm that methanol is produced on the β-PdZn alloy phase. Some catalysts make CH₄; however, β-PdZn is not responsible for CH₄ production. CH₄ was detected only on catalysts with the presence of TiO₂, either as support (Pd/TiO₂ and PdZn/TiO₂) or at the PdZn-support interface, that is, Pd/ZnTiO₃ converts to PdZn/ZnTiO₃, but with the support depleted of Zn (probably as TiO₂-like material). Thus, the metal there too may be supported on TiO₂. On PdZn-based catalysts CH₄ is produced as a decomposition product of methanol, which occurs both at the PdZn-TiO₂ interface and on TiO₂ surfaces, instead of through a CO₂ methanation mechanism on metal sites. In order to avoid CH₄ production as an undesired by-product, a support with no active sites for methanol degradation, such as ZnTiO₃, must be employed.

Associated Content

Support Information available: CO₂ hydrogenation data for synthesised catalyst at different temperatures, supports blank reactions and the physical mixture of Pd/ZnO with TiO₂. XRD pattern for commercial TiO₂, ZnO and synthesised ZnTiO₃, XRD patterns of prepared catalyst after annealing in static air (500 °C, 16 h) and XRD patterns after reduction in 5% H₂ (400 °C, 1 h), XPS Pd⁰, PdO and PdZn peak fitting parameters, Zn(2p) and Zn (LM₂) XPS spectra, TEM images and particle size histograms.

Acknowledgements

The authors would like to acknowledge the UK Catalysis Hub and the EPSRC for funding (EP/N010531/1) the presented research. We would like to specially acknowledge Dr. Robert D. Armstrong for the design and assembly of the CO₂ hydrogenation reactor.

Conflict of Interest

The authors declare no conflict of interest.

Keywords: CO₂ hydrogenation · methane · methanol · PdZn alloy · zinc titanate

- [1] P. C. K. Vesborg, T. F. Jaramillo, *RSC Adv.* **2012**, *2*, 7933–7947.
- [2] J. Rockström, W. Steffen, K. Noone, Å. Persson, F. S. Chapin III, E. F. Lambin, T. M. Lenton, M. Scheffer, C. Folke, H. J. Schellnhuber, B. Nykvist, C. A. de Wit, T. Hughes, S. van der Leeuw, H. Rodhe, S. Sörlin, P. K. Snyder, R. Costanza, U. Svedin, M. Falkenmark, L. Karlberg, R. W. Corell, V. J. Fabry, J. Hansen, B. Walker, D. Liverman, K. Richardson, P. Crutzen, J. A. Foley, *Nature* **2009**, *461*, 472–475.
- [3] J. Twidell, T. Weir, *Renewable energy sources*, Third edition, Routledge, London and New York, 2015.
- [4] G. Olsson, P. D. Lund, *Glob. Chall.* **2017**, *1*, 1700056.
- [5] R. Schlögl, *ChemSusChem* **2010**, *3*, 209–222.
- [6] J. Toyir, R. Miloua, N. E. Elkadri, M. Nawdali, H. Toufik, F. Miloua, M. Saito, *Proc. JMSM 2008 Conf.* **2009**, *2*, 1075–1079.
- [7] W.-J. Shen, K.-W. Jun, H.-S. Choi, K.-W. Lee, *Korean J. Chem. Eng.* **2000**, *17*, 210–216.
- [8] H. Yang, C. Zhang, P. Gao, H. Wang, X. Li, L. Zhong, W. Wei, Y. Sun, *Catal. Sci. Technol.* **2017**, *7*, 4580–4598.
- [9] S. G. Jadhav, P. D. Vaidya, B. M. Bhanage, J. B. Joshi, *Chem. Eng. Res. Des.* **2014**, *92*, 2557–2567.
- [10] E. V. Kondratenko, G. Mul, J. Baltrusaitis, G. O. Larrazábal, J. Pérez-Ramírez, *Energy Environ. Sci.* **2013**, *6*, 3112–3135.
- [11] J. Ma, N. Sun, X. Zhang, N. Zhao, F. Xiao, W. Wei, Y. Sun, *Spec. Int.* **2009**, *148*, 221–231.
- [12] J. Ereña, I. Sierra, M. Olazar, A. G. Gayubo, A. T. Aguayo, *Ind. Eng. Chem. Res.* **2008**, *47*, 2238–2247.
- [13] N. Iwasa, H. Suzuki, M. Terashita, M. Arai, N. Takezawa, *Catal. Lett.* **2004**, *96*, 75–78.
- [14] J. A. Rodríguez, *J. Phys. Chem.* **1994**, *98*, 5758–5764.
- [15] J. Díez-Ramírez, P. Sánchez, A. Rodríguez-Gómez, J. L. Valverde, F. Dorado, *Ind. Eng. Chem. Res.* **2016**, *55*, 3556–3567.
- [16] J. Díez-Ramírez, F. Dorado, A. R. de la Osa, J. L. Valverde, P. Sánchez, *Ind. Eng. Chem. Res.* **2017**, *56*, 1979–1987.
- [17] H. Bahruji, M. Bowker, G. Hutchings, N. Dimitratos, P. Wells, E. Gibson, W. Jones, C. Brookes, D. Morgan, G. Lalev, *J. Catal.* **2016**, *343*, 133–146.
- [18] V. Lebarbier, R. Dagle, A. Datye, Y. Wang, *Appl. Catal.* **2010**, *379*, 3–6.
- [19] J.-N. Park, E. W. McFarland, *J. Catal.* **2009**, *266*, 92–97.
- [20] W. Wei, G. Jinlong, *Front. Chem.* **2011**, *5*, 2–10.
- [21] J. Xu, X. Su, X. Liu, X. Pan, G. Pei, Y. Huang, X. Wang, T. Zhang, H. Geng, *Appl. Catal. A* **2016**, *514*, 51–59.
- [22] X.-L. Liang, X. Dong, G.-D. Lin, H.-B. Zhang, *Appl. Catal. B* **2009**, *88*, 315–322.
- [23] A. S. Malik, S. F. Zaman, A. A. Al-Zahrani, M. A. Daous, H. Driss, L. A. Petrov, *Appl. Catal.* **2018**, *560*, 42–53.
- [24] V. Arunajatesan, B. Subramaniam, K. W. Hutchenson, F. E. Herkes, *Chem. Eng. Sci.* **2007**, *62*, 5062–5069.
- [25] R. A. Dagle, A. Platon, D. R. Palo, A. K. Datye, J. M. Vohs, Y. Wang, *Appl. Catal.* **2008**, *342*, 63–68.
- [26] M. M. Forde, R. D. Armstrong, C. Hammond, Q. He, R. L. Jenkins, S. A. Kondrat, N. Dimitratos, J. A. Lopez-Sanchez, S. H. Taylor, D. Willock, C. J. Kiely, G. J. Hutchings, *J. Am. Chem. Soc.* **2013**, *135*, 11087–11099.
- [27] M. M. Forde, R. D. Armstrong, R. McVicker, P. P. Wells, N. Dimitratos, Q. He, L. Lu, R. L. Jenkins, C. Hammond, J. A. Lopez-Sanchez, C. J. Kiely, G. J. Hutchings, *Chem. Sci.* **2014**, *5*, 3603–3616.
- [28] M. M. Forde, L. Kesavan, M. I. bin Saiman, Q. He, N. Dimitratos, J. A. Lopez-Sanchez, R. L. Jenkins, S. H. Taylor, C. J. Kiely, G. J. Hutchings, *ACS Nano* **2014**, *8*, 957–969.
- [29] H. Bahruji, M. Bowker, W. Jones, J. Hayward, J. Ruiz Esquiús, D. J. Morgan, G. J. Hutchings, *Faraday Discuss.* **2017**, *197*, 309–324.
- [30] H. Bahruji, J. R. Esquiús, M. Bowker, G. Hutchings, R. D. Armstrong, W. Jones, *Top. Catal.* **2018**, *61*, 144–153.
- [31] J. H. Kwak, L. Kovarik, J. Szanyi, *ACS Catal.* **2013**, *3*, 2094–2100.
- [32] T. Szailer, É. Novák, A. Oszkó, A. Erdőhelyi, *Top. Catal.* **2007**, *46*, 79–86.
- [33] N. Iwasa, S. Masuda, N. Ogawa, N. Takezawa, *Appl. Catal.* **1995**, *125*, 145–157.
- [34] H. Bahruji, R. D. Armstrong, J. R. Esquiús, W. Jones, M. Bowker, G. J. Hutchings, *Ind. Eng. Chem. Res.* **2018**, *57*, 6821–6829.
- [35] L.-F. Liao, C.-F. Lien, D.-L. Shieh, M.-T. Chen, J.-L. Lin, *J. Phys. Chem. B* **2002**, *106*, 11240–11245.
- [36] H. Bahruji, M. Bowker, C. Brookes, P. R. Davies, I. Wawata, *Appl. Catal.* **2013**, *454*, 66–73.
- [37] N. Aas, T. J. Pringle, M. Bowker, *J. Chem. Soc. Faraday Trans.* **1994**, *90*, 1015–1022.
- [38] M. A. A. Aziz, A. A. Jalil, S. Triwahyono, A. Ahmad, *Green Chem.* **2015**, *17*, 2647–2663.
- [39] S. Penner, B. Jenewein, H. Gabasch, B. Klötzer, D. Wang, A. Knop-Gericke, R. Schlögl, K. Hayek, *J. Catal.* **2006**, *241*, 14–19.
- [40] M. W. Tew, H. Emerich, J. A. van Bokhoven, *J. Phys. Chem. C* **2011**, *115*, 8457–8465.
- [41] K. M. Eblagon, P. H. Concepción, H. Silva, A. Mendes, *Appl. Catal. B* **2014**, *154–155*, 316–328.
- [42] XPSsimplified.
- [43] L. S. Kibis, A. I. Titkov, A. I. Stadnichenko, S. V. Koscheev, A. I. Boronin, *Appl. Surf. Sci.* **2009**, *255*, 9248–9254.
- [44] M. Brun, A. Berthet, J. C. Bertolini, *J. Electron Spectrosc. Relat. Phenom.* **1999**, *104*, 55–60.

- [45] Y. Zhang, Y. Cai, Y. Guo, H. Wang, L. Wang, Y. Lou, Y. Guo, G. Lu, Y. Wang, *Catal. Sci. Technol.* **2014**, *4*, 3973–3980.
- [46] A. Baylet, P. Marécot, D. Duprez, P. Castellazzi, G. Groppi, P. Forzatti, *Phys. Chem. Chem. Phys.* **2011**, *13*, 4607–4613.
- [47] P. Kast, M. Friedrich, F. Girgsdies, J. Kröhnert, D. Teschner, T. Lunkenbein, M. Behrens, R. Schlögl, *Catal. Today* **2016**, *260*, 21–31.
- [48] M. Friedrich, D. Teschner, A. Knop-Gericke, M. Armbrüster, *J. Catal.* **2012**, *285*, 41–47.
- [49] C. Rameshan, W. Stadlmayr, C. Weilach, S. Penner, H. Lorenz, M. Hävecker, R. Blume, T. Rocha, D. Teschner, A. Knop-Gerike, R. Schlögl, N. Memmel, D. Zemlyanov, G. Rupprechter, B. Klöltzer, *Angew. Chem. Int. Ed.* **2010**, *49*, 3224–3227; *Angew. Chem.* **2010**, *122*, 3292–3296.
- [50] W. Li, L. Fang, G. Qin, H. Ruan, H. Zhang, C. Kong, L. Ye, P. Zhang, F. Wu, *J. Appl. Phys.* **2015**, *117*, 145301–145305.
- [51] G. Deroubaix, P. Marcus, *Surf. Interface Anal.* **1992**, *18*, 39–46.
- [52] S. Kuld, C. Conradsen, P. G. Moses, I. Chorkendorff, J. Sehested, *Angew. Chem. Int. Ed.* **2014**, *53*, 5941–5945; *Angew. Chem.* **2014**, *126*, 6051–6055.

Manuscript received: June 11, 2020
Revised manuscript received: September 4, 2020
Accepted manuscript online: September 14, 2020
Version of record online: October 14, 2020